AIAA JOURNAL
Vol. 35, No. 12, December 1997

Momentum Variable Procedure for Solving Compressible and Incompressible Flows

M. Darbandi* and G. E. Schneider†
University of Waterloo, Waterloo, Ontario N2L 3E5, Canada

Navier–Stokes equations are solved for both compressible and incompressible flows using momentum component variables instead of the usual velocity variables as the dependent variables. The numerical procedure is developed in a control-volume-based, finite element context. The procedure is determined in a pressure-based algorithm rather than the density-based algorithms, which compressible methods normally use. The proper selection of the connections between the variables on control volume surfaces and the main nodal values allow the use of a collocated grid arrangement. The compressible and incompressible results of this algorithm are investigated by testing a number of test cases including the driven cavity, an entrance region flow, and a converging–diverging nozzle flow. The results indicate that the momentum component procedure is quite successful for solving compressible and incompressible flows within a single algorithm.

Nomenclature

F, G, f, g	= momentum components at node and integration point (IP)
$\mathcal{F}, \mathcal{G}$	= convection fluxes
M	= Mach number
N_i	= finite element shape functions
P, p	= pressure at node and IP
$\boldsymbol{Q}, \boldsymbol{q}$	= conserve quantity vector at node and IP
R	= gas constant
$\mathcal{R}, \mathcal{T}$	= diffusion fluxes
Re	= Reynolds number
T	= temperature
t	= time
U, V, u, v	= velocity components at node and IP
$\mathcal{V}$	= the volume of control volume
x, y	= global Cartesian coordinates
μ	= viscosity
ρ	= density
τ	= stress tensor components

Subscript

ip	= IP values; Fig. 1

Superscripts

o	= previous time step value
$\bar{}$	= lagged from previous iteration

Introduction

THE idea of developing codes capable of solving both compressible and incompressible flows has been largely investigated in finite element, finite difference, and control-volume algorithms. Early attempts go back to the finite difference work of Harlow and Amsden,[1] whose scope of applicability is limited. Zienkiewicz and Wu[2] developed a general explicit and semiexplicit procedure; however, the use of the nonconservative form of the equations could result in different shock behavior than that involving full conservation. Chen and Pletcher[3] developed a finite difference-based algorithm for solving the time-dependent Navier–Stokes equations applicable to low Mach number flows.

Most of the control-volume-based methods for flow at all speeds return to the incompressible work of Patankar and Spalding,[4] SIMPLE, in which the continuity equation is considered as the constraint equation for pressure. Issa and Lockwood[5] extended a SIMPLE-based algorithm to solve compressible flow. Van Doormal et al.[6] used modified versions of SIMPLE to show that a pressure-based method can be extended to include compressible flows. The control-volume-based, finite difference method of Karki and Patankar[7] is also based on the compressible form of the SIMPLE algorithm for solving the steady-state form of the equations. Shyy et al.[8] also developed a similar procedure using a multigrid algorithm. All of these control-volume-based solvers are formulated on a staggered grid arrangement, which guarantees the coupling of velocity and pressure fields.[4,9] Contrary to a staggered grid arrangement, the collocated grid needs special treatment for the coupling of velocity and pressure. For example, Rhie and Chow[10] specified two velocity fields to suppress the decoupling problem. However, Schneider and Raw[11] used a collocated grid approach in their incompressible method, which considers the physical influence aspects of flow in integration point equations. Karimian and Schneider[12] proposed two velocity fields for the latter method to suppress the decoupling problem that could arise under special circumstances. They later extended their method for solving compressible flows.[13]

Generally, all of the methods mentioned use velocity components as the dependent variables. However, another choice is the momentum component, which may result in advantages such as extending an analogy that permits incompressible methods to be used to solve for compressible flows,[14] simplifying the linearization procedure, realizing fewer oscillations passing through a shock,[15] etc. Basically, most all-speed methods are extensions of incompressible methods to compressible flows.[6–8,13] Hence, they use the incompressible dependent variables, i.e., velocity components, to solve compressible flows. The idea of using momentum variables instead of velocity variables was firstly introduced by Darbandi and Schneider[16] for flows at all speeds. That implicit collocated approach is now extended and tested for solving two-dimensional flows.

Domain Discretization

We follow the collocated grid approach of Schneider and Raw,[11] which is control volume based (Fig. 1a). In this approach, nodes are located at the corners of the element and will be the locations of all problem unknowns. A local nonorthogonal coordinate system (ξ, η) is defined inside each element. Finite element shape functions will be used to relate the global and local coordinates to each other.

Received Nov. 18, 1995; presented as Paper 96-0605 at the AIAA 34th Aerospace Sciences Meeting, Reno, NV, Jan. 15–18, 1996; revision received July 16, 1997; accepted for publication Sept. 8, 1997.

*Postdoctoral Fellow, Department of Mechanical Engineering. Member AIAA.

†Professor, Department of Mechanical Engineering. Associate Fellow AIAA.

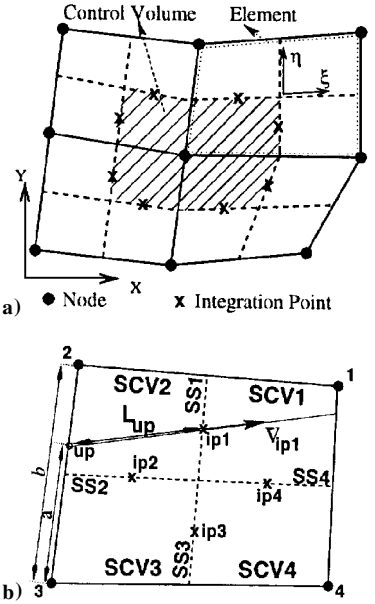

Fig. 1 Domain discretization and velocity upwinding.

Computational Modeling

Governing Equations

The desired governing equations are written as

$$\frac{\partial \boldsymbol{q}}{\partial t} + \frac{\partial \mathcal{F}(\boldsymbol{q})}{\partial x} + \frac{\partial \mathcal{G}(\boldsymbol{q})}{\partial y} = \frac{\partial \mathcal{R}(\boldsymbol{q})}{\partial x} + \frac{\partial \mathcal{T}(\boldsymbol{q})}{\partial y} \tag{1}$$

where $\boldsymbol{q} = (\rho, \rho u, \rho v, \rho e)^T$, $\mathcal{F} = (\rho u, \rho u^2 + p, \rho uv, \rho uh)^T$, $\mathcal{G} = (\rho v, \rho vu, \rho v^2 + p, \rho vh)^T$, $\mathcal{R} = (0, \tau_{xx}, \tau_{xy}, \sigma_x)^T$, and $\mathcal{T} = (0, \tau_{yx}, \tau_{yy}, \sigma_y)^T$. The components of the stress tensors are given by $\tau_{xx} = 2\mu u_x - \frac{2}{3}\mu(u_x + v_y)$, $\tau_{yy} = 2\mu v_y - \frac{2}{3}\mu(u_x + v_y)$, and $\tau_{xy} = \tau_{yx} = \mu(u_y + v_x)$. Here, σ_x and σ_y are the energy dissipation terms. The equation of state, $P = \rho RT$, is used to close the given system of equations. Alternatively, for the incompressible flow case the equation of state can be written as $\rho = \text{const}$.

Discretization of the Governing Equations

Equation (1) is integrated over four subcontrol volumes (SCV) of an element (Fig. 1). There are only two subsurfaces (SS) in each SCV that are considered in integration. Using the divergence theorem in Eq. (1) for SCV1 yields

$$\iiint_{\text{SCV1}} \frac{\partial \boldsymbol{q}}{\partial t}\,\mathrm{d}\mathcal{V} + \iint_{\text{SS1+SS4}} (\mathcal{F}\boldsymbol{i} + \mathcal{G}\boldsymbol{j})\cdot \mathrm{d}\boldsymbol{S} = \iint_{\text{SS1+SS4}} (\mathcal{R}\boldsymbol{i} + \mathcal{T}\boldsymbol{j})\cdot \mathrm{d}\boldsymbol{S} \tag{2}$$

where $\mathrm{d}\boldsymbol{S} = (\triangle S_x)\boldsymbol{i} + (\triangle S_y)\boldsymbol{j}$ is the normal vector to the surface. Because the method is fully implicit, all terms except the transient term are evaluated at the advanced time. The transient term is approximated by the nodal value of its corresponding node, i.e., $\iiint (\partial \boldsymbol{q}/\partial t)\,\mathrm{d}\mathcal{V} \approx J_{\text{SCV1}}(\boldsymbol{Q}_1 - \boldsymbol{Q}_1^o)/\triangle t$, where J is the Jacobian of transformation. Uppercase variables represent values at nodal points, and lowercase variables represent integration point values. The density is not a major dependent variable in $\boldsymbol{q}$ and needs to be treated properly for compressible flow. The equation of state is used to shift the active role of density to pressure in the continuity equation, $\rho = 1/(R\bar{T})P$. The integration of the convection flux terms yields

$$\iint_{\text{SS1+SS4}} (\mathcal{F}\boldsymbol{i} + \mathcal{G}\boldsymbol{j})\cdot \mathrm{d}\boldsymbol{S} = [\mathcal{F}_{\text{ip1}}(\triangle S_x)_{\text{SS1}} + \mathcal{F}_{\text{ip4}}(\triangle S_x)_{\text{SS4}}] + [\mathcal{G}_{\text{ip1}}(\triangle S_y)_{\text{SS1}} + \mathcal{G}_{\text{ip4}}(\triangle S_y)_{\text{SS4}}] \tag{3}$$

$\mathcal{F}$ and $\mathcal{G}$ are nonlinear in terms of momentum component variables and need linearization. At this stage, we simply linearize them to $\mathcal{F} \approx (f, \bar{u}f + p, \bar{u}g, \bar{f}h)^T$ and $\mathcal{G} \approx (g, \bar{v}f, \bar{v}g + p, \bar{g}h)^T$; however, there are other possible forms of linearization in the literature.[16]

The lagged velocities are calculated explicitly from known values of the preceding iteration, as is explained later. The integration of the diffusion flux terms of Eq. (2) yields

$$\iint_{\text{SS1+SS4}} (\mathcal{R}\boldsymbol{i} + \mathcal{T}\boldsymbol{j})\cdot \mathrm{d}\boldsymbol{S} = [\mathcal{R}_{\text{ip1}}(\triangle S_x)_{\text{SS1}} + \mathcal{R}_{\text{ip4}}(\triangle S_x)_{SS4}] + [\mathcal{T}_{\text{ip1}}(\triangle S_y)_{\text{SS1}} + \mathcal{T}_{\text{ip4}}(\triangle S_y)_{SS4}] \tag{4}$$

Stress terms in $\mathcal{R}$ and $\mathcal{T}$ are in terms of velocity components. Therefore, the following substitution reforms them to an appropriate form in terms of momentum variables, i.e., $\partial u/\partial x = (1/\rho)(\partial F/\partial x) - (u/\rho)(\partial \rho/\partial x)$. The second term on the right-hand side is calculated explicitly and treated as a source term. The first term is calculated using finite element shape functions. For the sake of brevity, the procedure is written for the $\partial u/\partial x$ case on SS1, i.e.,

$$\iint_{\text{SS1}} \left.\frac{\partial u}{\partial x}\right|_{\text{ip1}} \boldsymbol{i}\cdot \mathrm{d}\boldsymbol{S} \approx \left[\frac{1}{\bar{\rho}}\sum_{j=1}^{4}\frac{\partial N_j}{\partial x}(F_j - \bar{u}\bar{\rho}_j)\right]_{\text{ip1}} (\triangle S_x)_{\text{SS1}} \tag{5}$$

where $j = 1$–4 includes the influence of the nodal points at the four corners of each element.

Integration Point Equations

As the next step, unknown variables at integration points that appear in the conservation statements need to be connected to the nodal values of the element. These connections have been largely investigated in control-volume methods. The integration point pressure is simply approximated by using finite element shape functions, i.e.,

$$p_{\text{ip1}} = \sum_{j=1}^{4}(N_j)_{\text{ip1}} P_j$$

However, a good approximation for the convected velocity can be obtained by considering the physical interpretation of the governing equations in mathematical expressions. In this regard, Schneider and Raw[11] derive an algebraic approximation to the differential equations at each integration point that includes the physics and relevant couplings. Following their method for deriving integration point velocities, integration point momentums are derived by treating the nonconservative form of the momentum equations. In this regard, the momentum equations are written as

$$\frac{\partial f}{\partial t} + V_{\text{tot}}\frac{\partial f}{\partial s} - \mu\,\nabla^2 u = -\frac{\partial p}{\partial x} + \Pi + u\left(\frac{\partial \rho}{\partial t} + V_{\text{tot}}\frac{\partial \rho}{\partial s}\right) \tag{6}$$

$$\frac{\partial g}{\partial t} + V_{\text{tot}}\frac{\partial g}{\partial s} - \mu\,\nabla^2 v = -\frac{\partial p}{\partial y} + \Pi + v\left(\frac{\partial \rho}{\partial t} + V_{\text{tot}}\frac{\partial \rho}{\partial s}\right) \tag{7}$$

where $V_{\text{tot}} = \sqrt{(\bar{u}^2 + \bar{v}^2)}$ and Π is the remainder of viscous terms that are not considered at this point. Π has little importance in finding the correct integration point value. We derive the f_{ip} from Eq. (6). The transient term is written in backward form, $\partial f/\partial t \approx (f_i - f_i^o)/\triangle t$, where the subscript i denotes the integration point number. This model is also applied to the $\partial \rho/\partial t$ term on the right-hand side of Eq. (6) considering $\rho_i \approx \bar{\rho}_i$.

The convection terms are written in the streamwise direction, which provides the correct direction of upwinding. Hence, they are upwinded as $V_{\text{tot}}(\partial f/\partial s) \approx (V_{\text{tot}})_i(f_i - (f_{\text{up}})_i)/(L_{\text{up}})_i$. L_{up} and f_{up} are shown in Fig. 1b for integration point 1. Note f_{up} is interpolated between the two adjacent nodes, which are nodes 2 and 3 for integration point 1 in Fig. 1b, $(f_{\text{up}})_1 = (a/b)F_2 + (1 - (a/b))F_3$. This procedure is similarly applied to the $\partial \rho/\partial s$ term on the right-hand side of Eq. (6) considering $\rho_i \approx \bar{\rho}_i$ and $\rho_{\text{up}} \approx \bar{\rho}_{\text{up}}$. The pressure term in Eq. (6) is treated by

$$\frac{\partial p}{\partial x} \approx \sum_{j=1}^{4}\left(\frac{\partial N_j}{\partial x}\right)_i P_j$$

The role of the incompressible part of the diffusion term is considered as active in deriving f. Considering the elliptic nature of diffusion, the Laplacian operator is approximated by

$$\nabla^2 u = \nabla^2\left(\frac{f}{\rho}\right) \approx \left[\sum_{j=1}^{4} \frac{(N_j)_i}{\bar{\rho}_j} F_j - \left(\frac{f}{\bar{\rho}}\right)_i\right] \Big/ \left(L_d^2\right)_i \qquad (8)$$

where L_d is an appropriate diffusion length scale.[11] This approximation reduces to

$$f_i \approx \sum_{j=1}^{4} N_j F_j$$

when diffusion dominates the convection. The substitution of the models in Eq. (6) will finally yield

$$\{f\} = [C^{ff}]\{F\} + [C^{fp}]\{P\} + \{C^f\} \qquad (9)$$

where C^{ff} and C^{fp} are two 4×4 matrices, which indicate the effect of the F and P fields on f. C^f is a 4×1 known array. The first and second superscripts of the C indicate to which equation and parameter of equation it belongs, respectively. An expression similar to Eq. (9) could be similarly derived for g by starting from Eq. (7). It yields

$$\{g\} = [C^{gg}]\{G\} + [C^{gp}]\{P\} + \{C^g\} \qquad (10)$$

These integration point momentums are substituted into the momentum parts of the linearized $\mathcal{F}$ and $\mathcal{G}$. A similar procedure on the nonconservative form of the energy equation results in an expression for integration point temperature.

Mass Conserving Expressions

The expressions that we have already derived for f and g are called convected. These expressions are not suitable for substitution in the continuity equation because it may still result in the decoupling problem under certain conditions.[16] One remedy is to derive a second set of expressions for f and g. The idea of using two integration point values for a collocated grid arrangement goes back to the work of Rhie and Chow.[10] Darbandi and Schneider[16] derived a second integration point equation for the momentum component, which considers the numerical errors of both continuity and momentum equations at the integration point. To derive a second integration point value for f, a velocity weighted continuity-equation error is subtracted from Eq. (6). It is

$$\frac{\partial f}{\partial t} + V_{\text{tot}}\frac{\partial f}{\partial s} - \mu\nabla^2 u + \frac{\partial p}{\partial x} - \Pi - u\left(\frac{\partial \rho}{\partial t} + V_{\text{tot}}\frac{\partial \rho}{\partial s}\right) - u\left[\frac{\partial \rho}{\partial t} + \frac{\partial f}{\partial x} + \frac{\partial g}{\partial y}\right] = 0 \qquad (11)$$

All of the terms in the momentum part of this equation are treated as in the preceding section. The method of discretization for the second bracket is explained here. The $u(\partial\rho/\partial t)$ term is treated in the same manner as the similar term in Eq. (6). The two other terms are discretized using bilinear interpolation:

$$u_i\left(\frac{\partial f}{\partial x} + \frac{\partial g}{\partial y}\right)_i \approx \bar{u}_i\left[\sum_{j=1}^{4}\frac{\partial N_j}{\partial x}F_j + \sum_{j=1}^{4}\frac{\partial N_j}{\partial y}G_j\right]_i \qquad (12)$$

The substitution of these modelings into Eq. (11) finally results in

$$\{\hat{f}\} = [C^{\hat{f}f}]\{F\} + [C^{\hat{f}g}]\{G\} + [C^{\hat{f}p}]\{P\} + \{C^{\hat{f}}\} \qquad (13)$$

This new integration point expression is called the convecting mass for f. To distinguish it from the convected one, we use a caret on f, $\hat{f}$. A similar convecting expression could be derived for $\hat{g}$. These integration point expressions are substituted into the continuity equation. The lagged convecting velocities in our formulation are calculated based on the lagged values of these variables.

Results

Because the intent of this work is to demonstrate the procedure, a direct solver was used for the computations. Thus, it is not relevant to present computational times for solutions in this work. The solution always started with $F = G = 0$ for all nonboundary nodes. For more comprehensive results and discussions, the reader is referred to Ref. 17.

Cavity Flow Problem

The cavity problem is tested for $Re = 5 \times 10^3$ and 7.5×10^3. The length scale and density are considered to be unity. Figure 2 shows the streamline contours in the cavity with a grid resolution of 101×101. All of the first- and second-level vortices have been successfully detected despite using a relatively coarse grid. The velocity profiles at the centerlines are shown in Fig. 3. Figure 3 also demonstrates the results of mesh refinement studies and compares them with the benchmark results of Ghia et al.,[18] who use a fine-grid distribution of 257×257. The current results show an excellent agreement with the benchmark solution even using a coarse grid distribution.

Next, the details of the cavity flow are studied. Table 1 shows a comprehensive survey on the strengths, dimensions, and locations of the primary vortices inside the cavity with $Re = 5 \times 10^3$. Table 1 gives primary P, top T, bottom-left BL, and bottom-right BR vortices, where 1st represents the level of the vorticity in the primary vortex in each bottom corner and H and V represent the horizontal and vertical sizes of the vortex, respectively. The results demonstrate excellent quantitative agreement with the results of the benchmark solution.

Finally, the compressible cavity was investigated for many Reynolds numbers for which the results are identical to those of incompressible flow. There are reasons for such identical solutions.[17] Figure 4 shows the results at $Re = 1 \times 10^3$ for $M = 0.0033$ and 0.9

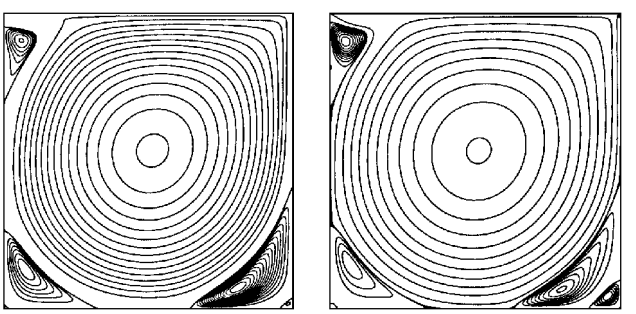

a) $Re = 5 \times 10^3$ b) $Re = 7.5 \times 10^3$

Fig. 2 Streamlines in cavity with 101×101 grid.

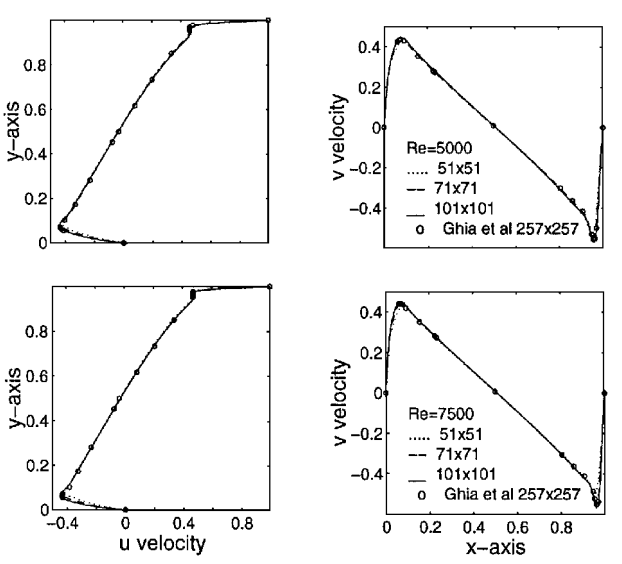

Vertical center line **Horizontal center line**

Fig. 3 Mesh refinement study in incompressible cavity with $Re = 5 \times 10^3$ and 7.5×10^3.

Table 1 Detail comparison of incompressible cavity flow results, $Re = 5 \times 10^3$

		Ghia et al.[18a]	This work[b]	Error, %
P	ψ_{min}	−0.11897	−0.1208	1.54
	x, y	0.512, 0.535	0.515, 0.535	0.59, 0.0
	ψ_{max}	1.456E−3	1.414E−3	2.91
T	x, y	0.063, 0.910	0.063, 0.9055	0.0, 0.49
	H, V	0.121, 0.269	0.1211, 0.268	0.08, 0.37
1st	ψ_{max}	1.361E−3	1.365E−3	0.29
BL	x, y	0.070, 0.137	0.07, 0.13	0.0, 5.11
	H, V	0.318, 0.264	0.317, 0.269	0.31, 1.9
1st	ψ_{max}	3.083E−3	3.146E−3	2.04
BR	x, y	0.809, 0.074	0.805, 0.0703	0.87, 5.00
	H, V	0.357, 0.418	0.3568, 0.411	0.06, 1.67

[a]With 257 × 257 grid distribution. [b]With 101 × 101 grid distribution.

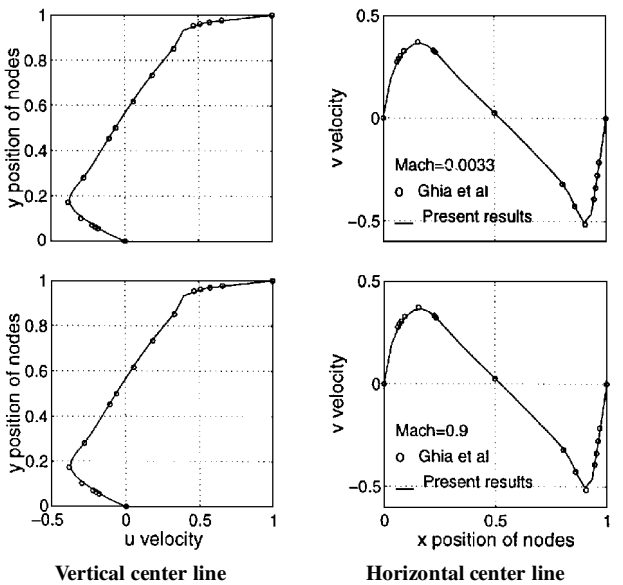

Fig. 4 Compressible cavity with $M \approx 0.0033$ and 0.9 and $Re = 1 \times 10^3$.

and compares them with those of the benchmark. The low Mach number of $M = 0.0033$ is obtained by considering unit velocity for the lid. This, of course, is not the lower limit for solving low Mach number flows.[14] This high flexibility of the method in solving very low Mach number flows as compressible flows is not available in extended compressible methods that solve incompressible flow.[19] Generally, the excellence of the agreement persists for all Mach numbers up to sonic speeds.

The cavity problem was studied as a steady-state problem, and the results of each case were obtained using several iterations with an extremely large time step. The number of iterations was between 10 and 20 in each case to satisfy an rms criterion of 10^{-5}.

Entrance Flow Problem

The second test problem is the entrance flow to a parallel plate duct. The schematic development of the velocity profiles in the entrance region shows a peculiar behavior close to the entrance.[17] Darbandi and Schneider[20] perform a comprehensive study on this problem. They show that the magnitude of the overshoots approaches a limit with refinement of the grid; however, the centerline velocity distribution is almost mesh independent. Figure 5 illustrates the progress of the centerline velocity for $Re = 20$. The results of the current method are compared with those of Morihara and Cheng,[21] who solve the quasilinear Navier–Stokes equations for incompressible flow. In addition, they are compared with the compressible results of Chen and Pletcher,[3] who solve for compressible and incompressible flows. Generally, all of the methods tend to similar distributions. However, Table 2 tabulates the convergence histories and compares the performance of the current method with that of Chen and Pletcher.[3] The grid distributions for $Re = 10$, 75, and 7.5×10^3 are 21×11, 31×11, and 41×11, respectively. As is seen,

Table 2 Iterations required to achieve the criterion in entrance flow, $M = 0.05$

Reynolds	10	75	7.5×10^3
Ref. 3	42	87	200
This work	3	3	3

Table 3 Developing flow length

Reynolds	This work[a]	Ref. 22	Ref. 21[b]
0	1.3	——	1.282
1	1.3	1.282	1.302
20	2.2	2.220	2.237
200	18.0	16.70	18.060
1×10^3	87.5	91.080	——
2×10^3	170.0	168.80	171.600

[a]With 101 × 21 grid distribution. [b]With 41 × 21 grid distribution.

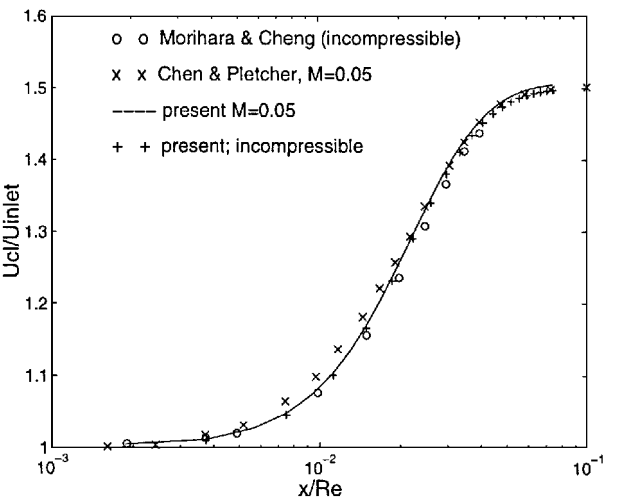

Fig. 5 Centerline velocity distribution in entrance region, $Re = 20$; U distribution on centerline grid.

the number of time steps to achieve the convergence criterion of 10^{-4} is significantly lower and more stable for the current method than that of Ref. 3.

Table 3 presents the computed developing length X_e and compares it with the results of the Refs. 21 and 22. X_e is defined as the distance from the inlet boundary, with uniform velocity profile, to the point where centerline velocity reaches 99% of the asymptotic value.[17] There is very good agreement despite using a coarse grid. To investigate the accuracy of the solution, the mesh size was changed from nonuniform 101×21 grid to uniform 61×21 grid distributions. The effect of mesh size was found to be small. The number of iterations for attaining the convergence criterion was lower by a factor of two for the lowest Reynolds number to six for the highest one.

Converging–Diverging Nozzle Flow

The last test case is a planar converging–diverging nozzle, which is solved for inviscid flow. The geometry of this symmetric nozzle is given by $y = \sqrt{(1 + 3x^2)}$, where $-1 \le x \le +1$ and $y \ge 0$, with a 10-fold stretch in the x direction. Back pressure and mass flow were specified downstream and upstream of the nozzle, respectively. Figure 6 shows the Mach number distributions at the centerline of the nozzle for a number of grids. The results are compared with the exact solution of the one-dimensional flow through a nozzle. As is seen, they show excellent agreement with the exact solution, although a finer grid generally results in a more accurate distribution.

Next, the problem is tested for mixed subsonic–supersonic flow. The grid distribution is 51×13. In this case, the exit pressure is selected in such a manner that a pressure ratio of $P_{exit}/(P_0)_{in} = 0.795$ produces shock at the section $A/A^* = 1.31$ with strength $M_1/M_2 = 2.575$. The results are shown in Fig. 7 and compared with the numerical and the one-dimensional exact solutions. The exact solution has

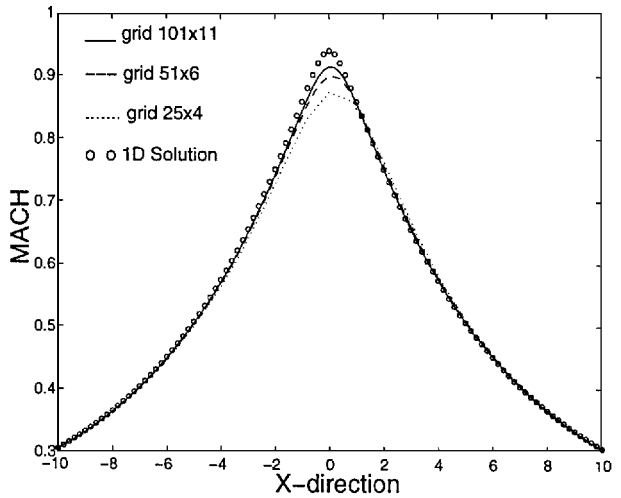

Fig. 6 Centerline Mach distribution for converging–diverging nozzle, $M_{throat} \approx 0.95$; mesh refinement study for subsonic nozzle flow.

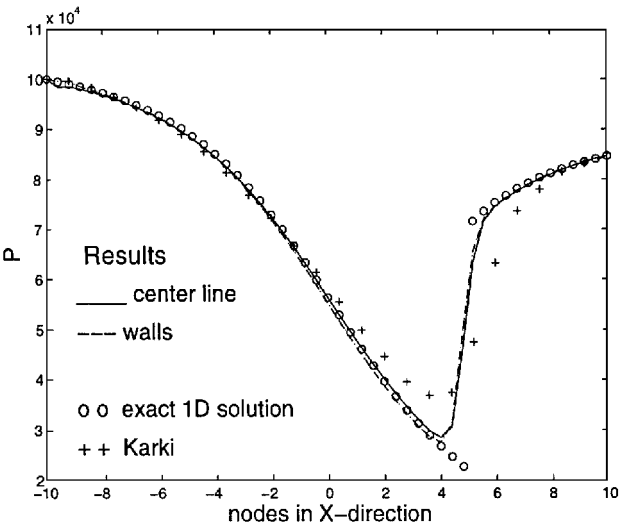

Fig. 7 Centerline pressure distribution and comparison for a nozzle with $M_{max} \approx 1.67$; P distribution for supersonic nozzle, isentropic.

been computed at the nodes, and these values are shown by circles. Karki[23] solves this test case using a quasi-one-dimensional algorithm. The ability of the current method to predict the location and the strength of the shock is notable. The smearing in the front of the shock is due to the integration point temperature calculation. On the other hand, the two dimensionality of the flow is another issue that may affect the agreement between the two solutions.[17] A total of 182 time steps were executed to achieve the rms iteration change of 10^{-5} for the dependent variables.

Conclusion

A new procedure was developed for solving compressible and incompressible flows. Momentum components, pressure, and temperature were selected as dependent variables in a control-volume-based method. Convected integration point equations were derived by treating the nonconservative form of the governing equations. Mass conserving equations were extended by the combination of momentum and continuity equation errors to completely suppress the decoupling problem. The incompressible and compressible parts of the algorithm were separately validated by solving cavity flow, entrance flow, and converging–diverging nozzle flow and comparing their results with those of benchmark solutions and with other workers' available results. The compressible part of the algorithm showed excellent performance in solving to very low Mach number flows. The robustness of the momentum component procedure in achieving reliable results even on coarse grids is noteworthy.

Acknowledgments

The authors thank the Natural Sciences and Engineering Research Council of Canada and the Ministry of Higher Education of Iran for their financial support of this work.

References

[1] Harlow, F. M., and Amsden, A. A., "A Numerical Fluid Dynamics Calculation Method for All Flow Speeds," *Journal of Computational Physics*, Vol. 8, Oct. 1971, pp. 197–213.

[2] Zienkiewicz, O. C., and Wu, J., "A General Explicit or Semi-Explicit Algorithm for Compressible and Incompressible Flows," *International Journal for Numerical Methods in Engineering*, Vol. 35, No. 3, 1992, pp. 457–479.

[3] Chen, K. H., and Pletcher, R. H., "Primitive Variable, Strongly Implicit Calculation Procedure for Viscous Flows at All Speeds," *AIAA Journal*, Vol. 29, No. 8, 1991, pp. 1241–1249.

[4] Patankar, S. V., and Spalding, D. B., "A Calculation Procedure for Heat, Mass, and Momentum Transfer in Three-Dimensional Parabolic Flows," *International Journal of Heat and Mass Transfer*, Vol. 15, Oct. 1972, pp. 1787–1806.

[5] Issa, R. I., and Lockwood, F. C., "On the Prediction of Two Dimensional Supersonic Viscous Interactions Near Walls," *AIAA Journal*, Vol. 15, No. 2, 1977, pp. 182–188.

[6] Van Doormal, J. P., Raithby, G. D., and McDonald, B. H., "The Segregated Approach to Predicting Viscous Compressible Fluid Flows," *Journal of Turbomachinery*, Vol. 109, No. 2, 1987, pp. 268–277.

[7] Karki, K. C., and Patankar, S. V., "Pressure Based Calculation Procedure for Viscous Flows at All Speeds in Arbitrary Configurations," *AIAA Journal*, Vol. 27, No. 9, 1989, pp. 1167–1173.

[8] Shyy, W., Chen, M. H., and Sun, C. S., "Pressure-Based Multigrid Algorithm for Flow at All Speeds," *AIAA Journal*, Vol. 30, No. 11, 1992, pp. 2660–2669.

[9] Raithby, G. D., and Schneider, G. E., "Numerical Solution of Problems in Incompressible Fluid Flow; Treatment of the Velocity-Pressure Coupling," *Numerical Heat Transfer*, Vol. 2, Dec. 1979, pp. 417–440.

[10] Rhie, C. M., and Chow, W. L., "Numerical Study of the Turbulent Flow Past an Airfoil with Trailing Edge Separation," *AIAA Journal*, Vol. 21, No. 11, 1983, pp. 1525–1532.

[11] Schneider, G. E., and Raw, M. J., "Control Volume Finite Element Method for Heat Transfer and Fluid Flow Using Co-located Variables—1. Computational Procedure," *Numerical Heat Transfer*, Vol. 11, No. 4, 1987, pp. 363–390.

[12] Karimian, S. M. H., and Schneider, G. E., "Numerical Solution of Two Dimensional Incompressible Navier–Stokes Equations: Treatment of Velocity-Pressure Coupling," AIAA Paper 94-2359, June 1994.

[13] Karimian, S. M. H., and Schneider, G. E., "Pressure Based Control-Volume Finite-Element Method for Flow at All Speeds," *AIAA Journal*, Vol. 33, No. 9, 1995, pp. 1611–1618.

[14] Darbandi, M., and Schneider, G. E., "Use of a Flow Analogy in Solving Compressible and Incompressible Flows," AIAA Paper 97-0706, Jan. 1997.

[15] Darbandi, M., and Schneider, G. E., "A Comparative Study of Velocity and Momentum in Pressure-Based Algorithm," *Proceedings of the Fifth Annual Conference of the CFD Society of Canada* (Victoria, BC, Canada), CFDSC, Ottawa, ON, Canada, 1997, pp. 3-35–3-41.

[16] Darbandi, M., and Schneider, G. E., "Momentum Component Variable Procedure for Flow at All Speeds," *Proceedings of the Third Annual Conference of the CFD Society of Canada* (Banff, AB, Canada), CFDSC, Ottawa, ON, Canada, 1995, pp. 145–156.

[17] Darbandi, M., and Schneider, G. E., "Solving Compressible and Incompressible Flows Using a Momentum Variable Calculation Procedure," AIAA Paper 96-0605, Jan. 1996.

[18] Ghia, U., Ghia, K. N., and Shin, C. T., "High-Re Solutions for Incompressible Flow Using the Navier–Stokes Equations and a Multigrid Method," *Journal of Computational Physics*, Vol. 48, No. 3, 1982, pp. 387–411.

[19] Volpe, G., "Performance of Compressible Flow Codes at Low Mach Numbers," *AIAA Journal*, Vol. 31, No. 1, 1993, pp. 49–56.

[20] Darbandi, M., and Schneider, G. E., "A Study of the Overshoots of the Entrance Flow Using Control Volume Method," *Proceedings of the Fourth Annual Conference of the CFD Society of Canada* (Ottawa, ON, Canada), CFDSC, Ottawa, ON, Canada, 1996, pp. 219–227.

[21] Morihara, H., and Cheng, R. T., "Numerical Solution of Viscous Flow in the Entrance Region of Parallel Plates," *Journal of Computational Physics*, Vol. 11, No. 4, 1973, pp. 550–572.

[22] Narang, B. S., and Krishnamoorthy, G., "Laminar Flow in Entrance Region of Parallel Plates," *Journal of Applied Mechanics*, Vol. 43, March 1976, pp. 186–188.

[23] Karki, K. C., "A Calculation Procedure for Viscous Flows at All Speeds in Complex Geometries," Ph.D. Dissertation, Dept. of Mechanical Engineering, Univ. of Minnesota, Minneapolis, MN, June 1986.

D. S. McRae
Associate Editor